Frontiers of Physics
https://doi.org/10.1007/s11467-018-0863-2
Front. Phys.
14(1), 13609 (2019)

RESEARCH ARTICLE

Majorana fermions in semiconducting nanowire and Fulde–Ferrell superconductor hybrid structures

Jia Liu[1,2,†], **Chun Fai Chan**[2], **Ming Gong**[2,3,‡]

[1] *Guangdong Provincial Key Laboratory of Quantum Engineering and Quantum Materials, and School of Physics and Telecommunication Engineering, South China Normal University, Guangzhou 510006, China*
[2] *Department of Physics and Center of Coherence, The Chinese University of Hong Kong, Shatin, N. T., Hong Kong, China*
[3] *Key Laboratory of Quantum Information, University of Science and Technology of China, Hefei 230026, China*
Corresponding authors. E-mail: [†]*liuj.phys@foxmail.com,* [‡]*gongm@ustc.edu.cn*
Received June 13, 2018; accepted August 14, 2018

The novel idea that spin-orbit coupling (SOC) and an s-wave pairing system can lead to induced p-wave pairing with a strong magnetic limit, has stimulated widespread interest in searching for Majorana fermions (MFs) in semiconductor-superconductor hybrid structures. However, despite major advances in the semiconductor nanotechnology, this system has several inherent limitations that prohibit the realization and identification of MFs. We overcome these limitations by replacing the s-wave superconductor with the type-II Fulde–Ferrell (FF) superconductor, in which the center-of-mass momentum of the Cooper pair renormalizes the in-plane Zeeman field and chemical potential. As a result, MFs can be realized in semiconductor nanowires with small values of the Landé g-factor and high carrier densities. The SOC strength directly influences the topological boundary; thus, the topological phase transition and associated MFs can be engineered by an external electric field. Theoretically, almost all semiconductor nanowires can be used to realize MFs by using the FF superconductor. However, we find that InP nanowire is more suitable for the realization of MFs compared to InAs and InSb nanowires. Thus, this new scheme can take full advantage of the semiconductor nanotechnology for the realization of MFs in semiconductor-superconductor hybrid structures.

Keywords Majorana fermion, topological transition, Pfaffian, FF-superconductor, hybrid structure

Majorana fermion (MF), a particle which is its own antiparticle [1, 2], is the basic building block for fault-tolerant topological quantum computation [3, 4], thus it has been intensively explored in solid materials [5–19] and ultracold degenerate Fermi gas [20–26] in the past years. This exotic particle has been predicted more than 80 years for neutrino in particle physics [2], however, its materialization with quasi-particles is always of great challenge in physics. Breakthrough was made in recent years by the novel idea that spin-orbit coupling (SOC) and s-wave pairing can lead to *induced* p-wave pairing at strong Zeeman field. This idea can be traced back to the work by Gorov and Rashba [27] in 2001 that the SOC (induced by inversion symmetry breaking) can induce mixed singlet (s-wave) and triplet (p-wave) pairing in non-centrosymmetric superconductors [17–19, 28–33]. This novel idea has motivated recent theoretical and experimental endeavors in the searching of MFs using semiconductor nanowires on the top of s-wave superconductors [9–13, 16, 18, 19] (see recent review [34, 35]), as well as the realization of topological superfluids in spin-orbit coupled degenerate Fermi gas [22–25]. Recently, some promising signatures [36–39], though still in heavy debates [40–42], have been reported in a number of experiments based on InAs and InSb nanowires. These substantial progresses pave a way for the realization of MFs and topological quantum computation. In this scheme, the topological phase can be reached when $V_z^2 > \mu^2 + \Delta^2$ [9–12, 22, 23, 43, 44], where V_z, μ and Δ are Zeeman splitting, chemical potential and s-wave pairing strength, respectively. Generally, it means that strong magnetic field is required to realize the MFs. There are several basic challenges in experiments to reach this topological phase. Firstly, the s-wave superconductors generally have very small critical magnetic field ($B_c \sim 1$ Tesla, which corresponds to Zeeman splitting ~ 0.1 meV for Landé $g = 2$) [45, 46]. The Zeeman splitting induced by the critical magnetic field is generally much smaller than V_z unless for nanowires with large Landé g factor. Here we do not take the orbital momentum quenching effect into account, which may suppress the g factor due to strong confinement [47]. In another word, most of the semiconductor nanowires (with small g) are not suitable for the realization of MFs. Secondly, even for InAs and InSb nanowires with large g factor, the chemical potential $|\mu| < |V_z|$ sets another upper bound for carrier density, which is generally very low due to the small effective

© Higher Education Press and Springer-Verlag GmbH Germany, part of Springer Nature 2019

mass of electron [48]. As a result, the fluctuating effect may become significant, which can destroy the topological phase. Finally, the topological boundary is determined by the Hamiltonian's symmetry at zero momentum (from the viewpoint of Pfaffian [49]), thus the SOC strength, effective mass and direction of Zeeman field do not directly influence the boundary. In particular, the chemical potential in semiconductor is pinned by the Fermi surface of superconductor in the semiconductor-superconductor hybrid structures [48] and cannot be tuned by external gate. Thus the Zeeman field serves as the *only* possible parameter to be tuned in experiments [36–39]. The above dilemmas are all linked with one another and are unlikely to be solved based on s-wave superconductors. So the great advances in semiconductor nanotechnology cannot be directly used in this new platform for the searching of MFs.

This paper is aimed to provide a possible solution to the above dilemmas. We show that *all* these limitations can be solved by replacing the s-wave superconductor with type-II Fulde–Ferrell (FF) superconductors [50], in which the Cooper pairs carry a finite center-of-mass momentum $\boldsymbol{Q}$. The basic idea is that: (i) The center-of-mass momentum $\boldsymbol{Q}$ plays the role of renormalizing both the in-plane Zeeman field and chemical potential. As a result, the MFs can be realized for semiconductor nanowires with small Landé g factor and high carrier density. (ii) The SOC strength directly influences the topological boundary, thus the topological phase transition and associated MFs can be tuned by an external electric field, although its chemical potential is still pinned by the Fermi surface of superconductor. (iii) Almost *all* the Zinc blende and Wurtzite semiconductor nanowires can be used to realize MFs in this new platform. In particular, we find that InP nanowire, in some aspects, is more suitable for the realization of MFs than InAs and InSb. Our new platform therefore can integrate the advances of semiconductor nanotechnology to realize and identify MFs in this hybrid structure. Recently the researches for realizing FFLO superconductor achieved great improvements that makes our new scheme more significant [51–54].

Our basic setup is schematically shown in Fig. 1(a). The nanowire is in proximity contact with a FF superconductor, which generally has extremely large critical magnetic field ($\sim$ 10–30 Tesla) [28–33], thus the MFs can still be observed at strong magnetic field. Due to proximity effect, the pairing order parameter in nanowire is identical to that in FF superconductors, i.e., $\Delta(\boldsymbol{x}) = \Delta \mathrm{e}^{\mathrm{i}\boldsymbol{Q}\cdot\boldsymbol{x}}$. This result has been confirmed by Green's function calculation [55]. So the Hamiltonian describe the hybrid structure reads as ($\hbar = 1$) [56–58]

$$\begin{aligned} H &= H_0 + V_{\mathrm{FF}}, \\ H_0 &= \frac{\boldsymbol{k}^2}{2m^*} - \mu + \alpha(\boldsymbol{\sigma}\times\boldsymbol{k})\cdot\hat{z} + g\mu_B \boldsymbol{B}\cdot\boldsymbol{\sigma}, \\ V_{\mathrm{FF}} &= \Delta \sum_{\boldsymbol{k}} c^\dagger_{\boldsymbol{k}+\frac{\boldsymbol{Q}}{2},\uparrow} c^\dagger_{-\boldsymbol{k}+\frac{\boldsymbol{Q}}{2},\downarrow} + \mathrm{h.c.}, \end{aligned} \tag{1}$$

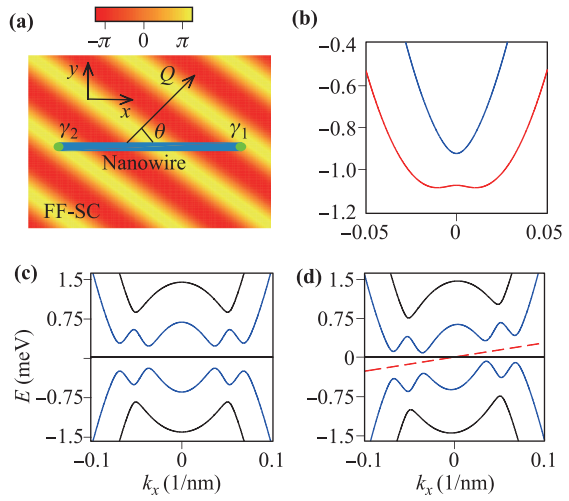


Fig. 1 **(a)** Semiconductor-FF superconductor hybrid structure for MFs. The phase modulation of the order parameter along direction θ is sketched by the color bar, and the Cooper pair center-of-mass momentum is denoted by $\boldsymbol{Q}$. The Zeeman field is assumed to along $\hat{x}$ direction. **(b)** Single particle band structure of the InP nanowire using the parameters from Table 1. **(c)** and **(d)** are typical band structures for $\boldsymbol{Q} = 0$ and $\boldsymbol{Q} = 0.01$/nm, respectively. Other parameters are $g\mu B_x = 0.38$ mV and $\theta = \pi/4$.

where m^* is the effective mass of electron, $\boldsymbol{k} = (k_x, k_y, k_z)$ is the electron momentum, $\boldsymbol{\sigma} = (\sigma_x, \sigma_y, \sigma_z)$ are the Pauli matrices, $\boldsymbol{B} = (B_x, B_y, B_z)$ is the external magnetic field and α is the Rashba SOC strength. $c^\dagger_{\boldsymbol{k},s}$ ($c_{\boldsymbol{k},s}$) is the creation (anihilation) operator with momentum $\boldsymbol{k}$ and spin s. The order parameter is set to real without lose of generality. Eq. (1) is obtained via a gauge transformation $c(\boldsymbol{x}) \to c(\boldsymbol{x})\mathrm{e}^{-\mathrm{i}\boldsymbol{Q}\cdot\boldsymbol{x}/2}$ in real space, where $\boldsymbol{Q}$ is the corresponding Cooper pair center-of-mass momentum. The corresponding Bogoliubov–de Gennes (BdG) equation reads

$$H_{\mathrm{BdG}}(\boldsymbol{k}) = \frac{\boldsymbol{k}\cdot\boldsymbol{Q}}{2m^*} + \begin{pmatrix} \bar{H}_0(\boldsymbol{k}) & \mathrm{i}\Delta\sigma_y \\ -\mathrm{i}\Delta\sigma_y & -\bar{H}_0^*(-\boldsymbol{k}) \end{pmatrix}, \tag{2}$$

in the Nambu basis $\Psi(\boldsymbol{k}) = (c_{\boldsymbol{k}+\boldsymbol{Q}/2,\uparrow}, c_{\boldsymbol{k}+\boldsymbol{Q}/2,\downarrow}, c^\dagger_{-\boldsymbol{k}+\boldsymbol{Q}/2,\uparrow}, c^\dagger_{-\boldsymbol{k}+\boldsymbol{Q}/2,\downarrow})^{\mathrm{T}}$. Here $\bar{H}_0(\boldsymbol{k}) = \frac{\boldsymbol{k}^2}{2m^*} - \bar{\mu} + \alpha(\boldsymbol{k}\times\boldsymbol{\sigma})\cdot\hat{z} + g\mu_B\bar{\boldsymbol{B}}\cdot\boldsymbol{\sigma}$, with $\bar{\mu} = \mu - \frac{|\boldsymbol{Q}|^2}{8m^*}$, $\bar{B}_x = B_x + \alpha Q_y/(2g\mu_B)$, $\bar{B}_y = B_y - \alpha Q_x/(2g\mu_B)$ and $\bar{B}_z = B_z$ [56]. Define the particle-hole operator as $\Theta = \tau_x K$, where τ_x is Pauli matrix acts on particle-hole space and K denotes the complex conjugation. We can verify that $\Theta H_{\mathrm{BdG}}(\boldsymbol{k})\Theta^{-1} = -H_{\mathrm{BdG}}(-\boldsymbol{k})$, so this system belongs to topological class D with topological index Z_2 [76].

The decoupling in Eq. (2) is exact in free space. The chemical potential is balanced out in part by the kinetic energy of Cooper pairs. For typical values $\boldsymbol{Q} \sim 0.05$–0.2/nm, we can estimate the kinetic energy of Cooper pair in InP nanowire to be about 0.30–4.72 meV. This large kinetic energy enables the realization of MFs at relative

large carrier density, in which the renormalized $\bar{\mu}$ can still be very small. The center-of-mass momentum also renormalizes the in-plane Zeeman fields. Using typical SOC strength, we can estimate that the Zeeman splitting induced by center-of-mass momentum to be the order of 0.5–2.0 meV, which is equivalent to $\boldsymbol{B} \sim$ 10–30 Tesla for typical semiconductor nanowires with small g factors. As a result, the required Zeeman splitting is not necessary to be provided by external Zeeman field and the Landé g factor has not to be large in this new platform. Notice that the SOC, as a standard technique in semiconductor nanotechnology, can be tuned by an external electric field. These estimations comprise the key idea of this work. Although in the following we mainly demonstrate our basic idea with InP nanowire [77, 78], in Fig. 3 we will summarize the major results using different conventional Zinc blende and Wurtzite semiconductor nanowires listed in Table 1.

We first consider a nanowire with strong confinement along its transverse direction, thus $\langle k_y \rangle = 0$ and $\langle k_z \rangle = 0$. The contribution of $\langle k_y^2 \rangle$ and $\langle k_z^2 \rangle$ can be absorbed into the chemical potential μ when only the lowest band along the transverse direction is occupied, i.e., single-band approximation. In this case the topological phase of Eq. (1) is determined by $\mathrm{Pf}(H_{\mathrm{BdG}}(k=0)\tau_x) = -1$, which yields

$$\bar{\mu}^2 + \Delta^2 < |g\mu_B \boldsymbol{B}|^2 + \alpha(g\mu_B \boldsymbol{B} \times \boldsymbol{Q}) \cdot \hat{e}_z + \frac{\alpha^2 |\boldsymbol{Q}|^2}{4}. \quad (3)$$

We can recover the well-known result in s-wave superconductor, $|g\mu_B \boldsymbol{B}|^2 > \mu^2 + \Delta^2$ [9–12, 22, 23], by setting $\boldsymbol{Q} = 0$. Here we see that the boundary is determined not only by the parameters in conventional s-wave superconductor (μ, Δ and $|g\mu_B \boldsymbol{B}|$), but also on the direction of external magnetic field, SOC strength and effective mass of Cooper pairs. These new parameters provide more knobs in experiments. In the weak SOC limit, $\boldsymbol{Q}$ only renormalizes the chemical potential. However, in the strong SOC limit, we have $\bar{\mu}^2 + \Delta^2 < \alpha(g\mu_B \boldsymbol{B} \times \boldsymbol{Q}) \cdot \hat{e}_z + \alpha^2 |\boldsymbol{Q}|^2/4 \sim \alpha^2 |\boldsymbol{Q}|^2/4$, which is independent of Landé g factor. Notice that the SOC strength is determined by inversion symmetry, thus can be easily controlled in experiments using an external electric field [79–81]. For this reason, the topological phase transition can be driven by an external electric field, although the chemical potential is still pinned by the Fermi surface of superconductor [48]. In other words, the advances in semiconductor nanotechnology can still be utilized in this hybrid structure to facilitate the realization and identification of MFs.

To gain a basic insight to this problem, we first present the different phases in Fig. 2(a). The interplay beween topology and energy gap gives rise to four different phases labeled by I to IV [82], where the gapped topological phase in regime I is what needed to search MFs. In Fig. 2(b), we have fixed all the other parameters but assumed $\boldsymbol{Q}$ can rotate in the plane with fixed magnitude. For small $\boldsymbol{Q}$ the system is gapped, however, for large $\boldsymbol{Q}$ it becomes gapless phase. The most special point in this work is that when $\boldsymbol{Q}$ is along y direction ($\boldsymbol{Q} \perp \boldsymbol{B}$), in which condition $\boldsymbol{k} \cdot \boldsymbol{Q} = 0$ and $(\boldsymbol{B} \times \boldsymbol{Q}) \cdot \hat{e}_z$ becomes maximum at $\theta = \pi/2$ and minimal at $\theta = 3\pi/2$ [see Fig. 2(c)]. In this case, we can exactly prove that the system is always gapped except at the critical point [83]. There is a small window when $\boldsymbol{Q}$ is not exactly perpendicular to the external magnetic field that still supports gapped topological phase [see Figs. 2(c) and (d)], and this small window can be controlled in experiments. We have verified that the system is always gapped when $\Delta^2 > \bar{h}_y^2$, thus the small window can be enlarged

Table 1 Parameters for typical Zinc blende and Wurtzite nanowires used in this work. In the first column the effective mass m^* is in unit of rest electron mass m_0, SOC strength α is in unit of meV·nm, $\Delta_{\mathrm{so}} = \alpha^2 m^*/2$ is in unit of μeV. The parameters for m^*, α are from Refs. [59–67] and the parameters for Landé g factor is from Refs. [68–75].

	Zinc blende						Wurtzite	
	InSb	InAs	GaSb	GaAs	InP	Si/Ge	GaN	AlN
m^*	0.014	0.026	0.04	0.063	0.08	0.19	0.15	0.25
α	10.0	15.0	10.0	5.0	5.0	0.06	0.55	0.55
Δ_{so}	9.0	38.0	26.0	10.0	13.0	0.004	0.3	0.5
g	−50.0	−15.0	−9.0	−0.4	1.3	−0.43	−2.1	1.0

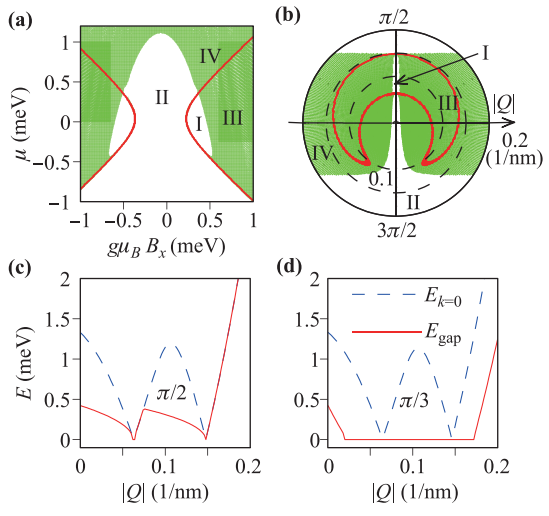


Fig. 2 **(a)** Phase diagram as a function of in-plane Zeeman field $\boldsymbol{B} = B\hat{x}$ and chemical potential for InP nanowire. The left and right parabolas (red lines) are topological boundary determined by Eq. (5). The colored and uncolored regimes correspond to gapless phase and gapped phase, respectively. $\boldsymbol{Q} = 0.02$/nm and $\theta = \pi/4$ are used. **(b)** Phase diagram in $\boldsymbol{Q}$ plane for fixed $\mu = 1$ meV and $g\mu_B B_x = 0.38$ meV. In both figures, I and III are gapped and gapless topological phase, while II and IV correspond to trivial gapped and gapless phase, respectively. **(c)** and **(d)** plot the energy gap at $k = 0$, and fundamental gap $E_{\mathrm{gap}} = \min|E_{n\boldsymbol{k}}|$, i.e., the minimal absolute energy gap of the total band structure, as a function of $\boldsymbol{Q}$. (c) and (d) correspond the result in (b) for $\theta = \pi/2$ and $\theta = \pi/3$.

by strong pairing. Moreover, we find that the system can always be gapped when $\bar{h}_x$ (or equivalently Q_y) exceeds some critical values, thus we have the stripe-like gapless region in Fig. 2(b). Generally, the small regime I can be greatly enlarged by a suitable choice of effective mass as well as SOC strength.

We have also examined the results by taking the multi-bands along the transverse direction into account. In the simplest case with two bands, the effective Hamiltonian reads as [84]

$$H_{\mathrm{BdG}}(\boldsymbol{k}) = H_0'\left(\boldsymbol{k}+\frac{\boldsymbol{Q}}{2}\right)\frac{1+\tau_z}{2} - H_0'^{*}\left(-\boldsymbol{k}+\frac{\boldsymbol{Q}}{2}\right)\frac{1-\tau_z}{2} - \sigma_y(\rho_x|\Delta_{12}| + \Delta_+ + \rho_z\Delta_-)\tau_y, \quad (4)$$

where $H_0'(\boldsymbol{k}) = H_0(\boldsymbol{k}) + E_{\mathrm{sp}}\frac{1-\rho_z}{2} - E_{\mathrm{bm}}\sigma_x\rho_y$, with $E_{\mathrm{sp}} = 3\pi^2/(2mL_y^2)$ is the subband energy difference, and $E_{\mathrm{bm}} = 8\alpha/(3L_y)$ is the band mixing energy, which corresponds to the expectation value $\hat{p}_y$ operator between different band eigenstates, ρ_i is the Pauli matrix acts on band degree. $\Delta_\pm = (\Delta_{11} \pm \Delta_{22})/2$, where Δ_{ij} defines pairing strength between band i and j. Notice that the system tends to become gapless phase when chemical potential is very large [56], thus only the lowest parabola can support gapped MFs although there are two different parabolas for topological phase. This regime can be realized for a small nanowire with relative large effective mass in experiments. The possible quenching of g factor is not important here [47].

The basic observations in Fig. 2 are quite general. In Fig. 3, we plot the possible $\boldsymbol{Q}$ (parallel the y direction) that can support gapped topological phase in different conventional semiconductor nanowires(see Table 1). Figure 3(a) are plotted based on initial condition $\boldsymbol{Q} = 0$ to be a trivial phase while Fig. 3(b) is plotted with initial condition to be topological phase. For different nanowires, we use their true effective mass and SOC as input parameters (see Table 1) for fixed chemical potential and Zeeman splitting $g\mu_B B_x$. These results clearly demonstrate that in almost all the semiconductors, the topological gapped FF phase can always be realized in a wide range of $\boldsymbol{Q}$. Especially, we find that InP nanowire which has relative large effective mass and weak SOC strength, in some aspects, is more suitable for the realization of MFs. This result is in stark contrast to the widely accepted belief that the MFs can only be realized in InAs or InSb nanowires due to their large Landé g factors [9–12, 36–39]. In this paper we only consider pure nanowires for simplicity, while in realistic experiments, it is possible to optimize the MFs by considering the alloyed nanowires, in which all the parameters in Table 1 can be tuned continually.

The major advantage of this new platform is that we can utilize the advances of semiconductor nanotechnology to engineer topological phase transition, although the chemical potential is still pinned by the Fermi surface of superconductor due to proximity effect [48]. The basic idea relies on the fact that the SOC strength is proportional to

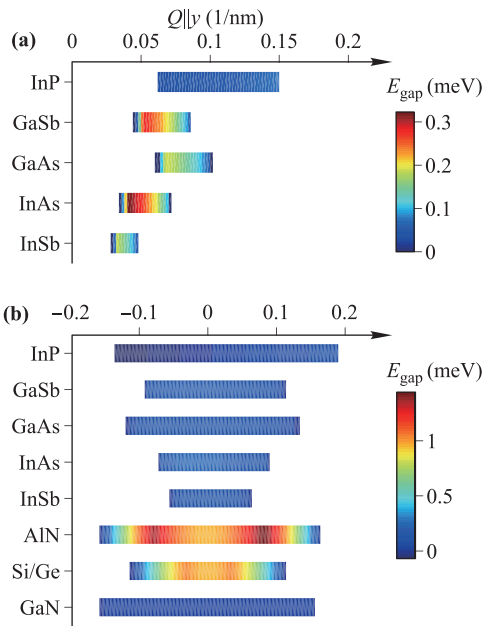


Fig. 3 Possible $\boldsymbol{Q} = Q\hat{y}$ for gapped topological phase. **(a)** $g\mu_B B_x = 0.38$ meV and **(b)** $g\mu_B B_x = 1.5$ meV. In both figures, $\Delta = 0.3$ meV and E_{gap} defines the minimal gap of the superconductors (see definition in caption of Fig. 2).

the external electric field [79–81], thus can be tuned in a wide range in realistic experiments. This result opens the possibility to engineer the topological phase transition and associated MFs using external electric field instead of magnetic field [36–39]. The results are demonstrated in Fig. 4. In Fig. 4(a), we show the influence of SOC strength ($\boldsymbol{Q}||y$) to the gapped trivial phase and gapped topological phase. We show that the SOC strength can dramatically modify the phase diagrams. Particularly, the gapped topological phase can be observed in a wide range of $\boldsymbol{Q}$ at strong SOC strength (the boundaries are composed by four different $\boldsymbol{Q}$ when α exceeds some critical values). Notice that the topological boundary cannot intersect with the $\boldsymbol{Q} = 0$ line, in which condition the topological boundary is independent of SOC strength. As a result, we find that the two gapped phase at strong SOC are always separated by a trivial phase. The SOC is also possible to drive the system from the gapless phase to the gapped topological phase when $\boldsymbol{Q}$ is not along y direction exactly, see Fig. 4(b). The results in Figs. 4(a) and (b) show that the gapped phase can be dramatically enlarged by controlling the direction of $\boldsymbol{Q}$ and the SOC strength.

We also study a realistic system with length $L_x = 3.0$ μm. We assume the wavefunction to be $\psi = (u_\uparrow, u_\downarrow, v_\downarrow, v_\uparrow)$, where u and v are expanded with plane wave basis with a sufficient large cutoff. The basic numerical results are presented in Fig. 4(c), in which we see a pair of topological protected MFs (due to Z_2 invariant) emerge exactly at the topological phase regime. A typical energy levels in the topological nanowires are presented in Fig. 4(d). The wavefunctions of MFs are well localized

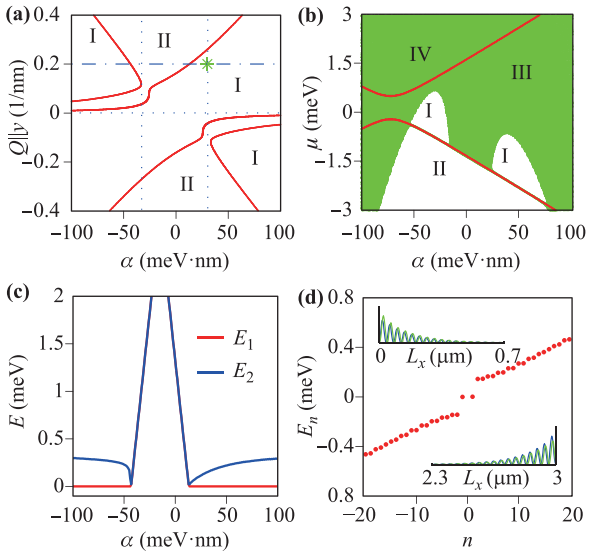


Fig. 4 **(a)** Phase diagram as a function of $\boldsymbol{Q}||y$ and SOC strength for $\mu = 1.0$ meV. When $|\alpha| \to \infty$, the two critical boundaries approach zero according to $Q \sim \frac{2}{\alpha}(-B_x \pm \sqrt{\Delta^2 + \mu^2})$, while the other two lines approach infinity according to $Q \sim \pm 4m\alpha$. **(b)** Phase diagram as a function of chemical potential and SOC strength for $|\boldsymbol{Q}| = 0.04$/nm, $\theta = 2\pi/5$. **(c)** and **(d)** consider a InP nanowire with length $L_x = 3.0$ μm in contact with a FF superconductor. In (c), we plot the lowest two non-negative eigenvalues E_1 and E_2 as a function of SOC strength for $\boldsymbol{Q}||y = 0.2$/nm [see dash-dotted line in (a)]. A typical energy levels at $\alpha = 30$ meV·nm [see the green star in (a)] is shown in (d), where the inset show the wave function of MFs. We have verified that $\gamma = \gamma^\dagger$ for the MFs. Throughout Fig. 4, $\Delta = 0.3$ meV and $g\mu_B B_x = 1.5$ meV.

at the two ends with exponential decay. The MFs can be denoted as $\gamma = \sum_{s=\uparrow,\downarrow} \int \mathrm{d}x u_s(x) c_s + v_s(x) c_s^\dagger$, where the self-hermitian, $\gamma = \gamma^\dagger$, requires that $u_s = v_s^*$, which is also verified in our numeric results.

The gapped topological phase depends strongly on the direction of $\boldsymbol{Q}$ and the best regime for this phase is $\boldsymbol{Q} \perp \boldsymbol{B}$. This condition can generally be fulfilled in real experiments. In the type-II FF superconductors, the center-of-mass momentum $\boldsymbol{Q}$ is generally produced by external magnetic field. For a non-centrosymmetric superconductor with Rashba SOC, it is well-known that the FF vector $\boldsymbol{Q} \perp \boldsymbol{B}$ [27, 85–88]. This basic conclusion also holds for contact (short range) interaction in ultracold atoms [89, 90]. Thus the small topological windows in Fig. 2 may be readily realized in this platform without further challenges. Notice that replacing the s-wave superconductor with type-II s-wave superconductor, which still has large critical field, do not have the above discussed advantages. It is worthwhile to emphasize that the braiding of MFs, in this new scheme, can also be achieved by a time-dependent spatial-varying electric field, which can tune the SOC strength hence the topological phase locally and adiabatically.

In summary, we show that the MFs can be elaborated with almost all conventional Zinc blende and Wurtzite semiconductors and FF superconductor hybrid structure. In this new platform the topological boundary depends on almost all the parameters of nanowires, thus it provides a lot of knobs for engineering topological phase transition. Together with the rapid development of the experiments for fabricating FFLO superconductor [41, 91], our new scheme shed light to the realization and identification of MFs in future experiments.

Acknowledgements We thank Z.-Y. Xue for helpful suggestions and discussions. This work was supported by the National Natural Science Foundation of China (Grant No. 11874156).

References and notes

1. F. Wilczek, Majorana returns, *Nat. Phys.* 5(9), 614 (2009)
2. E. Majorana, Teoria simmetrica dell'elettrone e del positrone, *Nuovo Cim.* 14(4), 171 (1937) (in Italian)
3. M. Z. Hasan and C. L. Kane, Topological insulators, *Rev. Mod. Phys.* 82(4), 3045 (2010)
4. X. L. Qi and S. C. Zhang, Topological insulators and superconductors, *Rev. Mod. Phys.* 83(4), 1057 (2011)
5. N. Read and D. Green, Paired states of fermions in two dimensions with breaking of parity and time-reversal symmetries and the fractional quantum Hall effect, *Phys. Rev. B* 61(15), 10267 (2000)
6. A. Y. Kitaev, Unpaired Majorana fermions in quantum wires, *Phys. Uspekhi* 44(10S), 131 (2001)
7. S. Das Sarma, M. Freedman, and C. Nayak, Topologically protected qubits from a possible non-Abelian fractional quantum Hall state, *Phys. Rev. Lett.* 94(16), 166802 (2005)
8. L. Fu and C. L. Kane, Superconducting proximity effect and Majorana fermions at the surface of a topological insulator, *Phys. Rev. Lett.* 100(9), 096407 (2008)
9. J. D. Sau, R. M. Lutchyn, S. Tewari, and S. Das Sarma, Generic new platform for topological quantum computation using semiconductor heterostructures, *Phys. Rev. Lett.* 104(4), 040502 (2010)
10. J. Alicea, Majorana fermions in a tunable semiconductor device, *Phys. Rev. B* 81(12), 125318 (2010)
11. Y. Oreg, G. Refael, and F. von Oppen, Helical liquids and Majorana bound states in quantum wires, *Phys. Rev. Lett.* 105(17), 177002 (2010)
12. R. Lutchyn, J. Sau, and S. Das Sarma, Majorana fermions and a topological phase transition in semiconductor-superconductor heterostructures, *Phys. Rev. Lett.* 105(7), 077001 (2010)
13. A. C. Potter and P. A. Lee, Multichannel generalization of Kitaev's Majorana end states and a practical route to realize them in thin films, *Phys. Rev. Lett.* 105(22), 227003 (2010)

14. J. Liu, Q. Han, L. B. Shao, and Z. D. Wang, Exact solutions for a type of electron pairing model with spin-orbit interactions and Zeeman coupling, *Phys. Rev. Lett.* 107(2), 026405 (2011)
15. T. H. Hsieh and L. Fu, Majorana fermions and exotic surface andreev bound states in topological superconductors: Application to $Cu_xBi_2Se_3$, *Phys. Rev. Lett.* 108(10), 107005 (2012)
16. L. Mao, M. Gong, E. Dumitrescu, S. Tewari, and C. W. Zhang, Hole-doped semiconductor nanowire on top of an s-wave superconductor: A new and experimentally accessible system for Majorana fermions, *Phys. Rev. Lett.* 108(17), 177001 (2012)
17. S. Nadj-Perge, I. K. Drozdov, J. Li, H. Chen, S. Jeon, J. Seo, A. H. MacDonald, B. A. Bernevig, and A. Yazdani, Observation of Majorana fermions in ferromagnetic atomic chains on a superconductor, *Science* 346(6209), 602 (2014)
18. E. J. H. Lee, X.-C. Jiang, M. Houzet, R. Aguado, C. M. Lieber, and S. De Franceschi, Spin-resolved Andreev levels and parity crossings in hybrid superconductor–semiconductor nanostructures, *Nat. Nanotechnol.* 9, 79 (2014)
19. M. T. Deng, S. Vaitiekėnas, E. B. Hansen, J. Danon, M. Leijnse, K. Flensberg, J. Nygård, P. Krogstrup, and C. M. Marcus, Majorana bound state in a coupled quantum-dot hybrid-nanowire system, *Science* 354(6319), 1557 (2016)
20. C. W. Zhang, S. Tewari, R. M. Lutchyn, and S. Das Sarma, $p_x + ip_y$ Superfluid from s-wave interactions of fermionic cold atoms, *Phys. Rev. Lett.* 101(16), 160401 (2008)
21. M. Sato and S. Fujimoto, Existence of Majorana fermions and topological order in nodal superconductors with spin-orbit interactions in external magnetic fields, *Phys. Rev. Lett.* 105(21), 217001 (2010)
22. M. Gong, S. Tewari, and C. W. Zhang, BCS-BEC crossover and topological phase transition in 3D spin-orbit coupled degenerate Fermi gases, *Phys. Rev. Lett.* 107(19), 195303 (2011)
23. M. Gong, G. Chen, S. T. Jia, and C. W. Zhang, Searching for Majorana fermions in 2D spin-orbit coupled fermi superfluids at finite temperature, *Phys. Rev. Lett.* 109(10), 105302 (2012)
24. H. Hu and X. J. Liu, Fulde–Ferrell superfluidity in ultracold Fermi gases with Rashba spin–orbit coupling, *New J. Phys.* 15(9), 093037 (2013)
25. X. J. Liu and H. Hu, Topological superfluid in one-dimensional spin-orbit-coupled atomic Fermi gases, *Phys. Rev. A* 85(3), 033622 (2012)
26. L. Jiang, T. Kitagawa, J. Alicea, A. R. Akhmerov, D. Pekker, G. Refael, J. I. Cirac, E. Demler, M. D. Lukin, and P. Zoller, Majorana fermions in equilibrium and in driven cold-atom quantum wires, *Phys. Rev. Lett.* 106(22), 220402 (2011)
27. L. P. Gor'kov and E. I. Rashba, Superconducting 2D system with lifted spin degeneracy: Mixed singlet-triplet state, *Phys. Rev. Lett.* 87(3), 037004 (2001)
28. I. Bonalde, W. Bramer-Escamilla, and E. Bauer, Evidence for line nodes in the superconducting energy gap of noncentrosymmetric $CePt_3Si$ from magnetic penetration depth measurements, *Phys. Rev. Lett.* 94(20), 207002 (2005)
29. N. Kimura, K. Ito, K. Saitoh, Y. Umeda, H. Aoki, and T. Terashima, Pressure-induced superconductivity in noncentrosymmetric heavy-fermion $CeRhSi_3$, *Phys. Rev. Lett.* 95(24), 247004 (2005)
30. I. Sugitani, Y. Okuda, H. Shishido, T. Yamada, A. Thamizhavel, E. Yamamoto, T. D. Matsuda, Y. Haga, T. Takeuchi, R. Settai, and Y. Ōnuki, Pressure-induced heavy-fermion superconductivity in antiferromagnet $CeIrSi_3$ without inversion symmetry, *J. Phys. Soc. Jpn.* 75(4), 043703 (2006)
31. H. Mukuda, T. Fujii, T. Ohara, A. Harada, M. Yashima, Y. Kitaoka, Y. Okuda, R. Settai, and Y. Onuki, Enhancement of superconducting transition temperature due to the strong antiferromagnetic spin fluctuations in the noncentrosymmetric heavy-fermion superconductor $CeIrSi_3$: A ^{29}Si NMR study under pressure, *Phys. Rev. Lett.* 100(10), 107003 (2008)
32. M. Nishiyama, Y. Inada, and G. Q. Zheng, Spin triplet superconducting state due to broken inversion symmetry in Li_2Pt_3B, *Phys. Rev. Lett.* 98(4), 047002 (2007)
33. S. K. Goh, Y. Mizukami, H. Shishido, D. Watanabe, S. Yasumoto, M. Shimozawa, M. Yamashita, T. Terashima, Y. Yanase, T. Shibauchi, A. I. Buzdin, and Y. Matsuda, Anomalous upper critical field in $CeCoIn_5/YbCoIn_5$ superlattices with a Rashba-type heavy fermion interface, *Phys. Rev. Lett.* 109(15), 157006 (2012)
34. J. Alicea, New directions in the pursuit of Majorana fermions in solid state systems, *Rep. Prog. Phys.* 75(7), 076501 (2012)
35. C. W. J. Beenakker, Search for Majorana fermions in superconductors, *Annu. Rev. Con. Mat. Phys.* 4(1), 113 (2013)
36. V. Mourik, K. Zuo, S. M. Frolov, S. R. Plissard, E. P. A. M. Bakkers, and L. P. Kouwenhoven, Signatures of Majorana fermions in hybrid superconductor-semiconductor nanowire devices, *Science* 336(6084), 1003 (2012)
37. M. T. Deng, C. L. Yu, G. Y. Huang, M. Larsson, P. Caroff, and H. Q. Xu, Anomalous zero-bias conductance peak in a Nb–InSb nanowire–Nb hybrid device, *Nano Lett.* 12(12), 6414 (2012)
38. A. Das, Y. Ronen, Y. Most, Y. Oreg, M. Heiblum, and H. Shtrikman, Zero-bias peaks and splitting in an Al–InAs nanowire topological superconductor as a signature of Majorana fermions, *Nat. Phys.* 8(12), 887 (2012)
39. L. P. Rokhinson, X. Y. Liu, and J. K. Furdyna, The fractional a.c. Josephson effect in a semiconductor–superconductor nanowire as a signature of Majorana particles, *Nat. Phys.* 8(11), 795 (2012)
40. T. D. Stanescu, S. Tewari, J. D. Sau, and S. Das Sarma, To close or not to close: The fate of the superconducting gap across the topological quantum phase transition in Majorana-carrying semiconductor nanowires, *Phys. Rev. Lett.* 109(26), 266402 (2012)

41. C. H. Lin, J. D. Sau, and S. Das Sarma, Zero-bias conductance peak in Majorana wires made of semiconductor/superconductor hybrid structures, *Phys. Rev. B* 86(22), 224511 (2012)
42. J. Liu, A. C. Potter, K. T. Law, and P. A. Lee, Zero-bias peaks in the tunneling conductance of spin-orbit-coupled superconducting wires with and without Majorana end-states, *Phys. Rev. Lett.* 109(26), 267002 (2012)
43. G. Ben-Shach, A. Haim, I. Appelbaum, Y. Oreg, A. Yacoby, and B. I. Halperin, Detecting Majorana modes in one-dimensional wires by charge sensing, *Phys. Rev. B* 91(4), 045403 (2015)
44. Y. X. Zeng, C. Lei, G. Chaudhary, and A. H. MacDonald, Quantum anomalous Hall Majorana platform, *Phys. Rev. B* 97(8), 081102 (2018)
45. D. K. Finnemore, D. E. Mapother, and R. W. Shaw, Critical field curve of superconducting mercury, *Phys. Rev.* 118(1), 127 (1960)
46. J. W. Rohlf, Modern Physics from A to Z, Wiley, 1994
47. C. E. Pryor and M. E. Flatte, Landé g factors and orbital momentum quenching in semiconductor quantum dots, *Phys. Rev. Lett.* 96(2), 026804 (2006)
48. M. Gong, L. Mao, S. Tewari, and C. W. Zhang, Majorana fermions under uniaxial stress in semiconductor-superconductor heterostructures, *Phys. Rev. B* 87, 060502(R) (2013)
49. P. Ghosh, J. D. Sau, S. Tewari, and S. Das Sarma, Non-Abelian topological order in noncentrosymmetric superconductors with broken time-reversal symmetry, *Phys. Rev. B* 82(18), 184525 (2010)
50. P. Fulde and R. A. Ferrell, Superconductivity in a strong spin-exchange field, *Phys. Rev.* 135(3A), A550 (1964)
51. G. Koutroulakis, H. Kühne, J. A. Schlueter, J. Wosnitza, and S. E. Brown, Microscopic study of the Fulde–Ferrell–Larkin–Ovchinnikov state in an all-organic superconductor, *Phys. Rev. Lett.* 116(6), 067003 (2016)
52. H. Maya, S. Krämer, M. Horvatić, C. Berthier, K. Miyagawa, K. Kanoda, and V. F. Mitrović, Evidence of Andreev bound states as a hallmark of the FFLO phase in κ-(BEDT-TTF)$_2$Cu(NCS)$_2$, *Nat. Phys.* 10, 928 (2014)
53. J. Wosnitza, FFLO states in layered organic superconductors, *Ann. Phys.* 530(2), 1700282 (2018)
54. Y. W. Guo and Y. Chen, Topological Fulde–Ferrell and Larkin–Ovchinnikov states in spin-orbit-coupled lattice system, *Front. Phys.* 13, 137402 (2018)
55. W. Chen, M. Gong, R. Shen, and D. Y. Xing, Detecting Fulde–Ferrell superconductors by an Andreev interferometer, *New J. Phys.* 16(8), 083024 (2014)
56. C. F. Chan and M. Gong, Pairing symmetry, phase diagram, and edge modes in the topological Fulde–Ferrell–Larkin–Ovchinnikov phase, *Phys. Rev. B* 89(17), 174501 (2014)
57. C. L. Qu, Z. Zheng, M. Gong, Y. Xu, L. Mao, X. B. Zou, G. C. Guo, and C. W. Zhang, Topological superfluids with finite-momentum pairing and Majorana fermions, *Nat. Commun.* 4(1), 2710 (2013)
58. W. Zhang and W. Yi, Topological Fulde–Ferrell–Larkin–Ovchinnikov states in spin–orbit-coupled Fermi gases, *Nat. Commun.* 4(1), 2711 (2013)
59. I. Vurgaftman, J. R. Meyer, and L. R. Ram-Mohan, Band parameters for III–V compound semiconductors and their alloys, *J. Appl. Phys.* 89(11), 5815 (2001)
60. J. P. Heida, B. J. vanWees, J. J. Kuipers, T. M. Klapwijk, and G. Borghs, Spin-orbit interaction in a two-dimensional electron gas in a InAs/AlSb quantum well with gate-controlled electron density, *Phys. Rev. B* 57(19), 11911 (1998)
61. V. A. Guzenko, A. Bringer, J. Knobbe, H. Hardtdegen, and Th. Schäpers, Rashba effect in $Ga_xIn_{1-x}As$/InP quantum wire structures, *Appl. Phys. A Mater. Sci. Process.* 87(3), 577 (2007)
62. W. A. Zein, N. A. Ibrahim, and A. H. Phillips, Spin polarized transport in an AC-driven quantum curved nanowire, *Phys. Res. Int.* 2011, 505091 (2011)
63. Th. Schäpers, V. A. Guzenko, A. Bringer, M. Akabori, M. Hagedorn, and H. Hardtdegen, Spin–orbit coupling in $Ga_xIn_{1-x}As$/InP two-dimensional electron gases and quantum wire structures, *Semicond. Sci. Technol.* 24(6), 064001 (2009)
64. J. G. Powles, B. Holtz, and W. A. B. Evans, New method for determining the chemical potential for condensed matter at high density, *J. Chem. Phys.* 101(9), 7804 (1994)
65. Z. Wilamowski, W. Jantsch, H. Malissa, and U. Rössler, Evidence and evaluation of the Bychkov–Rashba effect in SiGe/Si/SiGe quantum wells, *Phys. Rev. B* 66(19), 195315 (2002)
66. J. Luo, H. Munekata, F. F. Fang, and P. J. Stiles, Observation of the zero-field spin splitting of the ground electron subband in GaSb-InAs-GaSb quantum wells, *Phys. Rev. B* 38, 10142(R) (1988)
67. S. Lamari, Rashba effect in inversion layers on p-type InAs MOSFET's, *Phys. Rev. B* 64(24), 245340 (2001)
68. K. L. Litvinenko, L. Nikzad, C. R. Pidgeon, J. Allam, L. F. Cohen, T. Ashley, M. Emeny, W. Zawadzki, and B. N. Murdin, Temperature dependence of the electron Landé g factor in InSb and GaAs, *Phys. Rev. B* 77(3), 033204 (2008)
69. M. Oestreich and W. Rühle, Temperature dependence of the electron Landé g factor in GaAs, *Phys. Rev. Lett.* 74(12), 2315 (1995)
70. R. Zielke, F. Maier, and D. Loss, Anisotropic g factor in InAs self-assembled quantum dots, *Phys. Rev. B* 89(11), 115438 (2014)
71. S. Åsbrink and A. Waśkowska, Pressure-induced critical behavior of $KMnF_3$ close to $P_c = 3.1$ GPa: X-ray diffraction results, *Phys. Rev. B* 53, 12 (1996)
72. C. Hermann and C. Weisbuch, $\vec{k} \cdot \vec{p}$ perturbation theory in III-V compounds and alloys: A reexamination, *Phys. Rev. B* 15(2), 823 (1977)

73. Z. W. Zheng, B. Shen, Y. S. Gui, Z. J. Qiu, C. P. Jiang, N. Tang, J. Liu, D. J. Chen, H. M. Zhou, R. Zhang, Y. Shi, Y. D. Zheng, S. L. Guo, J. H. Chu, K. Hoshino, and Y. Arakawa, Enhancement and anisotropy of the Landau g factor in modulation-doped $Al_{0.22}Ga_{0.78}N$/GaN heterostructures, *J. Appl. Phys.* 95(5), 2473 (2004)

74. F. Maier, C. Klöffel, and D. Loss, Tunable g factor and phonon-mediated hole spin relaxation in Ge/Si nanowire quantum dots, *Phys. Rev. B* 87, 161305(R) (2013)

75. H. Kosaka, A. Kiselev, F. Baron, K. W. Kim, and E. Yablonovitch, Electron g factor engineering in III-V semiconductors for quantum communications, *Electron. Lett.* 37(7), 464 (2001)

76. A. P. Schnyder, S. Ryu, A. Furusaki, and A. W. W. Ludwig, Classification of topological insulators and superconductors in three spatial dimensions, *Phys. Rev. B* 78(19), 195125 (2008)

77. J. F. Wang, M. S. Gudiksen, X. F. Duan, Y. Cui, and C. M. Lieber, Highly polarized photoluminescence and photodetection from single indium phosphide nanowires, *Science* 293(5534), 1455 (2001)

78. K. Storm, F. Halvardsson, M. Heurlin, D. Lindgren, A. Gustafsson, P. M. Wu, B. Monemar, and L. Samuelson, Spatially resolved Hall effect measurement in a single semiconductor nanowire, *Nat. Nanotechnol.* 7(11), 718 (2012)

79. D. Liang and X. P. A. Gao, Strong tuning of spin orbit interaction in an InAs nanowire by surrounding gate, *Nano Lett.* 12, 6 (2012)

80. J. Nitta, T. Akazaki, H. Takayanagi, and T. Enoki, Gate control of spin-orbit interaction in an inverted $In_{0.53}Ga_{0.47}As/In_{0.52}Al_{0.4}As$ heterostructure, *Phys. Rev. Lett.* 78(7), 1335 (1997)

81. X. W. Zhang and J. B. Xia, Rashba spin-orbit coupling in InSb nanowires under transverse electric field, *Phys. Rev. B* 74(7), 075304 (2006)

82. The topological gapless phase III is still topological protected because it is impossible to adiabatically tune this phase to a trivial phase without closes the energy gap at zero momentum, see Ref. [56].

83. $\mathrm{Det}H_{\mathrm{BdG}}(k_x) = A^2 + \alpha^2 k_x^2$, where $A = \bar{h}_x^2 + \bar{h}_y^2 - k^4/(4m^{*2}) - \Delta^2 - \bar{\mu}^2 + k^2(\alpha^2 + \mu/m^*)$, so the energy gap can close only at the critical boundary; see also discussion in Ref. [22].

84. R. M. Lutchyn, T. D. Stanescu, and S. Das Sarma, Search for Majorana fermions in multiband semiconducting nanowires, *Phys. Rev. Lett.* 106(12), 127001 (2011)

85. S. K. Yip, Two-dimensional superconductivity with strong spin-orbit interaction, *Phys. Rev. B* 65(14), 144508 (2002)

86. D. F. Agterberg, Novel magnetic field effects in unconventional superconductors, *Physica C* 387(1–2), 13 (2003)

87. O. Dimitrova and M. V. Feigel'man, Theory of a two-dimensional superconductor with broken inversion symmetry, *Phys. Rev. B* 76(1), 014522 (2007)

88. D. F. Agterberg and R. P. Kaur, Magnetic-field-induced helical and stripe phases in Rashba superconductors, *Phys. Rev. B* 75(6), 064511 (2007)

89. Z. Zheng, M. Gong, X. B. Zou, C. W. Zhang, and G. C. Guo, Route to observable Fulde-Ferrell-Larkin-Ovchinnikov phases in three-dimensional spin-orbit-coupled degenerate Fermi gases, *Phys. Rev. A* 87(3), 031602 (2013)

90. Z. Zheng, M. Gong, Y. C. Zhang, X. B. Zou, C. W. Zhang, and G. C. Guo, FFLO superfluids in 2D spin-orbit coupled Fermi Gases, *Sci. Rep.* 4(1), 6535 (2015)

91. A. I. Larkin and Y. N. Ovchinnikov, Nonuniform state of superconductors, *Zh. Eksp. Teor. Fiz.* 47, 1136 (1964)